AUT Journal of Mechanical Engineering

AUT J. Mech. Eng., 4(1) (2020) 127-148
DOI: 10.22060/ajme.2019.14979.5754

Effect of Stator Dynamics on the Chaotic Behavior of Rotor-Disk-Bearing System under Rub-Impact between Disk and Stator

A. Rahi*, A. Haghanir, P. Safarpour

Faculty of Mechanical & Energy Engineering, Shahid Beheshti University, Tehran, Iran.

ABSTRACT: In the present study, the effect of stator dynamics on the chaotic behavior of a rotor-disk-bearing system with rub-impact between disk and stator is investigated. The governing equations of motion are derived using Jeffcott model and Newton's second law and then are made dimensionless. In the beginning, the system is modeled regardless of stator dynamics, and then the stator dynamics is also considered in the modeling of the system. In both cases, the system behavior is studied by bifurcation diagrams, time series diagrams, phase plane diagrams, power spectrum diagrams, Poincaré maps, and maximum Lyapunov exponent, respectively. The obtained results show that the type of stator dynamics modeling has a significant effect on the prediction of the response of a disk-bearing system with rub-impact between disk and stator. In other words, the results show the system has a chaotic behavior without considering the dynamics of the stator in mathematical modeling, while in the case of considering the stator dynamics and using the suitable values for the stator stiffness, the motion behavior of the system can be changed from the chaotic to the regular and periodic motion.

Review History:

Received: 15 Sep. 2018
Revised: 8 Apr. 2019
Accepted: 5 May. 2019
Available Online: 11 May. 2019

Keywords:

Rotor-disk-bearing
Stator dynamics
Rub-impact
Chaotic behavior

1- Introduction

Rub-impact in the rotating shaft is a secondary defect caused by a main defect in the system vibrations. The studies have shown that the reduction of radial looseness clearance in the seals is significant to increase the efficiency in turbomachinery such as steam turbines. Generally, in the rotating shaft system, increased efficiency is achieved by reducing the clearance between the fixed and rotary components. If the rotating shaft is not operating normally due to unbalancing, blade failures, lack of alignment, reduction of radial clearance, instabilities of the oil film and etc., there will probably be a rub-impact between fixed and rotary components. In the rotating shaft system, after fatigue failures, the rub-impact is the most important factor of damage. Though rubbing creates complex vibrations behavior, it is classified depending on the severity of the collision (full or partial rub), the direction of vibration response related to the rotation of the rotor in forward or backward whirling motion, or intense rub-impact. Today based on industrial and scientific studies available, main effects and characteristics of the different regimes of rub-impact in machines are well known .As in many cases, rubbing significantly changes the vibration behavior of the rotor-disk-bearing system, with online conditioning monitoring, could easily be fault detected.

In most of the previous studies, the rotary systems have been modeled using a simple Jeffcott rotor to study rub-impact between disk and stator without considering stator dynamics. Using this simple model, many researchers have studied the effect of various parameters such as rotor stiffness, rotor mass, damping of rotor and stator, the coefficient of friction between the contact surfaces, the amount of looseness and also different rotational speeds on the occurrence and persistence of the phenomenon of rubbing, theoretically and experimentally.

Muzyska [1] proposed a comprehensive discussion of the rubbing phenomenon as well as its effects on vibrations behavior of the rotating system. Khanloo et al. [2] studied the vibration analysis of a rotor-disk continuous chaotic system containing a flexible rotating rotor as well as rub-impact between the disk and the fixed component of the system. They modeled the system as a continuously rotating shaft with a rigid disk in the middle by including the effect of centrifugal and Coriolis forces. Khanloo et al. [3] investigated the effect of lateral–torsional coupling on the behavior of nonlinear dynamics of a continuous shaft-disk system. They studied the effect of coupled lateral and torsional on the chaotic behavior of the system.

Choi [4] considered partial rubbing due to contacting the rotor with a fixed component experimentally. He used two analytical models and showed that in the modeling of vibrations response of the system, the results of the linear model are good enough for this phenomena. Chu and Lu [5] studied the effect of the stiffness of the rotor during its contact with the stator in rotating machines. Shen et al. [6] investigated nonlinear rub-impact effect behavior of a bearing-rotor system with initial parameters rotor bow. They modeled the rotor-bearing system properly and the nonlinear forces

*Corresponding author's email: a_rahi@sbu.ac.ir

of oil films of journal bearings. Xiang et al. [7] investigated the nonlinear dynamics of an asymmetric rotor-disk-bearing system under rub-impact effect and also studied nonlinear force affecting the oil film. They proposed a mathematical model for a non-symmetric two disks rotor-bearing system with respect to oil film nonlinear force and rub-impact force. Also, they indicated that the dynamic behavior of the nonlinear system depends on rotational speeds.

Choy and Padovan [8] showed that with the increase of misalignment, the friction forces increase. They found that friction is the main cause of reverse rotation. Bartha [9] presented theoretical and experimental results on an opposite dry whip. He mentioned that at more than critical speeds, the friction force is stronger than damping force and leads to whip accelerating. Zhang and Meng [10] used basic models of Jeffcott micro-rotors and simple models of contact and Coulomb friction to study nonlinear dynamics and bifurcation theory for rub phenomenon in a high-speed rub-impact rotor system. They showed that increasing rotational speed causes intermittent motion changes to quasi-periodic and then finally chaotic motion. Roques et al. [11] modeled a turbo generator system with radial rubbing. They studied rubbing between the rotor and the stator that may be caused by a sudden misalignment. Goldman et al. [12], according to experimental results showed that during the transient motion of startup or shutdown, dry rotor whip inside mechanical seals occurs spontaneously and friction has a significant effect. In fact, as lubrication is applied to contact surfaces, the dry whip does not occur. Pavlovskaia et al. [13] used a simple Jeffcott model to study the stator preloading effect on the system response theoretically and experimentally. Feng and Zhang [14] examined rotor and stator vibration along with a primary disturbance. They used a simple Jeffcott model and a fixed stator model to study the system. Hall and Mba [15] used acoustic emissions approach for a rotor-stator rubbing in turbines to detect faults rotary machinery. Ma et al. [16] studied the analysis of dynamic characteristics of the rotor-stator system with assuming different rub-impact models. Chang-Jian et al. [17] investigated the non-linear dynamic response of a rub-impact rotor with two journal bearings. They used from assumption turbulent lubricant flow for the supported short journal bearings. Jeng et al. [18] studied the non-linear dynamic behavior of a rub-impact rotor system by response integration method to analyze chaotic behavior of the system response.

Xiang et al. [7] investigated the nonlinear dynamic response of a double-disk rotor-bearing system with rub-impact in the presence of oil-film forces. Hu et al. [19] studied the nonlinear dynamic behavior of an asymmetric double-disk rotor-bearing system with considering rub-impact and oil-film instability by numerical and experimental methods. Xiang et al. [20] investigated the instability of a rotor-bearing system with coupling rub-impact and crack faults under nonlinear oil-film force. They used a model considering time-varying crack stiffness, nonlinear oil-film force, and rub-impact force to analyze the complicated nonlinear responses of the rotor-bearing system. They showed that the crack depth and the stator stiffness have influences on the instability and vibration of the rotor-bearing system with the variation of rotating speed. Chen et al. [21] presented a new model to simulate the rub-impact contact force between the stator and rotating shell in the rotor system. They derived a formulation for the shell deformation and the relation between the contact region, deformation and forces.

Tofighi-Niaki et al. [22] used the mixed lubrication theory along with elasto-plastic asperity contact model between pads and journal to simulate rub–impact between the journal and the associated pads. They studied various dynamic behaviors of the rotor when the control parameters are changed by Phase plane orbits, waterfall frequency response spectra, Poincaré maps, and bifurcation diagrams. Prabith et al. [23] presented a modified model reduction method for the rub-impact behavior of a rotor-disk-stator system. The stability and bifurcation analysis of a nonlinear rotor system subjected to the rub-impact phenomenon and constant excitation were investigated by Hou et al. [24]. They formulated the harmonic balance method combined with an alternating frequency/time domain procedure to derive the approximate periodic solutions of the system. Moreira et al. [25] studied the nonlinear dynamic behavior of a non-smooth rotor system subjected to friction during contact between stator and rotor. They modeled the rub-impact between rotor and stator as an elastic interaction, subjected to Coulomb friction. Also, they used from the fourth-order Runge-Kutta method to solve the differential equations of motion. Hong et al. [26] investigated the nonlinear dynamic behaviors of a rotor system with an additional constraint due to rub-impact using the complex nonlinear modes. They derived the governing equation of motion, considering the modified Jeffcott rotor theory and the rub-impact between rotor and stator. In addition, they showed that by increasing the amplitude of the mode motion, the magnitudes of the modal frequencies, for both the forward and backward whirl, increase.

According to the previous researches, the effect of stator dynamics parameters on the motion behavior of a rotor-disk-bearing system with considering rub-impact between disk and stator have not been investigated. Therefore, the main contribution of the present paper is the study of stator dynamics effect on the motion behavior of a rotor-disk-bearing system with rub-impact between disk and stator. The results show that with considering the stator dynamics and using suitable values for the main parameters of the stator dynamics, the motion behavior of the system will change from chaotic motion to a regular and periodic motion.

In the present article, the effect of the stator dynamics on a rotor-disk-bearing system vibration behavior under rub-impact between disk and stator is studied. The rub-impact force is considered regarding elastic radial force and Coulomb tangential friction force in the governing equations of motion. Moreover, unbalance force and initial bow of the rotor which caused rub-impact between disk and stator, is considered. At first, the system without taking into account the stator dynamics under rub-impact is modeled and examined by system identification tools. Then in new modeling, dynamics of the stator is also considered in governing equations and is analyzed and evaluated the system again. The results show although the system has a chaotic behavior without regarding the stator dynamics, with considering the stator dynamics and using suitable values for stiffness of the stator, the motion behavior of the system will change from chaotic motion to a regular and periodic motion.

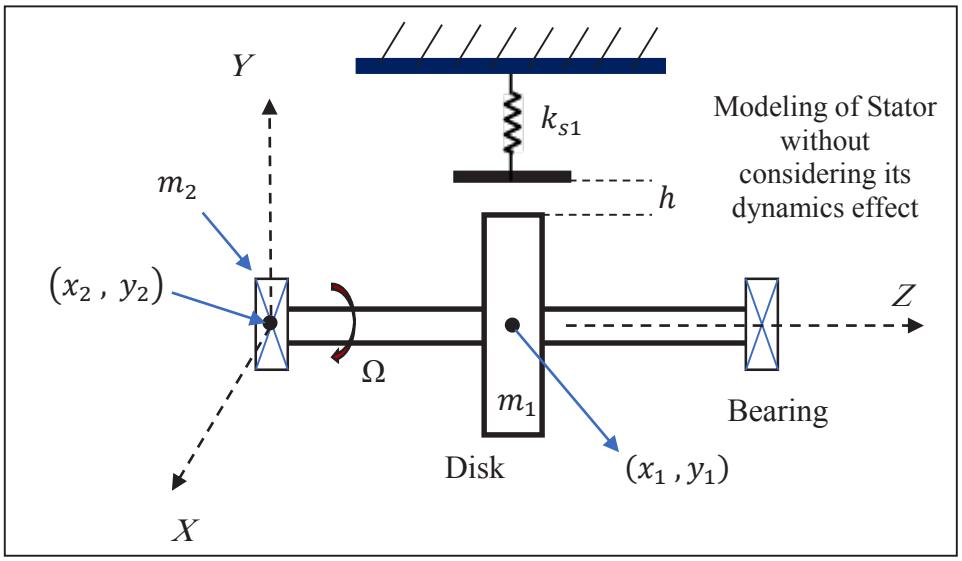

Fig. 1. Schematic model of a rotor-disk-bearing system without considering the stator dynamics effect

2- Modeling of a Rotor-Disk-Bearing System under Rub-Impact Between Disk and Stator

2- 1- Modeling of the system without considering stator dynamics

Fig. 1 shows the modeling of a schematic of the rotor-disk-bearing system under rub-impact without considering the stator dynamics. A rigid disk with mass m_1, radius R, mass eccentricity e_m is mounted in the middle of a flexible massless rotating shaft having stiffness k between the two short journal bearings. The rotating shaft has transverse stiffness k and rotational speed $\Omega\left(\frac{\text{rad}}{\text{s}}\right)$ which has been shown in Fig. 1.

In this modeling, the stator is taken as an additional stiffness while its dynamic is not considered. Term h is the radial clearance between the disk and the stator. Rotating shaft has an initial curvature r_0 of the geometric center (initial rotor bow). The displacement of the disk center and the displacement of the journal bearing center are (x_1, y_1) and (x_2, y_2), respectively. Following assumptions are also considered:

- The system has a viscous damping meaning damping is proportional to velocity.
- Gyroscopic effects are not considered.
- The transverse vibration of the system is considered only.
- The equivalent of the rotating shaft can be added to the m_1.

Governing equations of motion of the system can be derived using Jeffcott model and Newton's second law. At discrete modeling, the shaft is considered massless so the governing equations can be written only to disk and bearings in two directions x and y, as follows [7,17]:

$$\begin{aligned}
&m_1\ddot{x}_1 + c_1\dot{x}_1 + k\left(x_1 - x_2\right) = \Delta \cdot F_x\left(x_1, y_1\right) \\
&\quad + m_1 e_m \Omega^2 \cos\left(\Omega t\right) + k r_0 \cos\left(\Omega t - \beta\right) \\
&m_1\ddot{y}_1 + c_1\dot{y}_1 + k\left(y_1 - y_2\right) = \Delta \cdot F_y\left(x_1, y_1\right) \\
&\quad + m_1 e_m \Omega^2 \sin\left(\Omega t\right) + k r_0 \sin\left(\Omega t - \beta\right) - m_1 g \\
&m_2\ddot{x}_2 + c_2\dot{x}_2 + \frac{k}{2}\left(-x_1 + x_2\right) = p_x\left(x_2, y_2\right) \\
&m_2\ddot{y}_2 + c_2\dot{y}_2 + \frac{k}{2}\left(-y_1 + y_2\right) = p_y\left(x_2, y_2\right) - m_2 g
\end{aligned} \tag{1}$$

where β is the angle between unbalance and the bending, $F_x\left(x_1, y_1\right)$ and $F_y\left(x_1, y_1\right)$ are rubbing forces between the disk and the stator, c_1 and c_2 are damping coefficient of the rotating shaft and journal bearing, m_1 is the mass of the disk, m_2 is the mass of the journal bearing, g is the acceleration of gravity, and Ä is defined as follows:

$$\Delta = \begin{cases} 0 & if \quad r \le h \\ 1 & if \quad r > h \end{cases} \tag{2}$$

$$r = \sqrt{x_1^{\,2} + y_1^{\,2}}$$

Also, $p_x\left(x_2, y_2\right)$ and $p_y\left(x_2, y_2\right)$ are components of the oil film nonlinear forces that their values can be calculated as follows [7]:

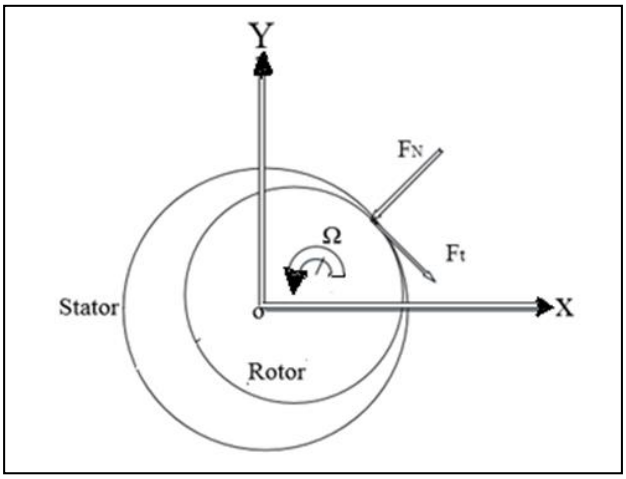

Fig. 2. Modelling of the rubbing forces

$$p_x\left(x_2,y_2\right)=-\mu\Omega RL\left(\frac{R}{c}\right)^2\left(\frac{L}{2R}\right)^2 \times\left[\frac{\sqrt{\left(x_2-2\dot{y}_2\right)^2+\left(x_2+2\dot{x}_2\right)^2}}{1-x_2^2-y_2^2}\right] \times\left[3xV\ -\sin\left(\beta\right)G-2\cos\left(\beta\right)Q\right] \tag{3}$$

$$p_y\left(x_2,y_2\right)=-\mu\Omega RL\left(\frac{R}{c}\right)^2\left(\frac{L}{2R}\right)^2 \times\left[\frac{\sqrt{\left(x_2-2\dot{y}_2\right)^2+\left(x_2+2\dot{x}_2\right)^2}}{1-x_2^2-y_2^2}\right] \times\left[3xV\ +\cos\left(\beta\right)G-2\sin\left(\beta\right)Q\right]$$

where

$$\beta=tan^{-1}\left(\frac{y_2+2\dot{x}_2}{x_2-2\dot{y}_2}\right)-\frac{\pi}{2}\left[\sin\left(\frac{y_2+2\dot{x}_2}{x_2-2\dot{y}_2}\right)+\sin\left(y_2+2\dot{x}_2\right)\right]$$

$$V\ =\frac{2+\left(y_2cos\beta-x_2sin\beta\right)G}{1-x_2^2-y_2^2} \tag{4}$$

$$G=\frac{2}{\sqrt{1-x_2^2-y_2^2}}\left[\frac{\pi}{2}+tan^{-1}\left(\frac{y_2cos\beta-x_2sin\beta}{1-x_2^2-y_2^2}\right)\right]$$

$$Q=\frac{x_2cos\beta-y_2sin\beta}{1-\left(x_2cos\beta-y_2sin\beta\right)^2}$$

where μ is the oil viscosity, and R, c, and L are the radius, the clearance, and the length of the journal bearing, respectively.

The mathematical modeling of rubbed effect between the rigid disk and the stator can be modeled according to Fig. 2 to obtain the contact forces.

Therefore, the contact forces between the disk and the stator can be obtained as follows [18]:

$$F_x\ =-F_N\ \cos\left(\phi\right)+F_t\ \sin\left(\phi\right)=-\left(1-\frac{h}{r}\right)k_{s1}\left(x_1-fy_1\right)$$

$$F_y\ =-F_N\ \sin\left(\phi\right)-F_t\ \cos\left(\phi\right)=-\left(1-\frac{h}{r}\right)k_{s1}\left(fx_1+y_1\right) \tag{5}$$

$$r=\sqrt{x_1^{\ 2}+y_1^{\ 2}}$$

where f denotes the coefficient of friction between the disk and the stator in rub-impact, k_{s1} denotes stator stiffness, F_N denotes the radial impact force, F_t denotes tangential rubbing force. In order to have Eq. (1) dimensionless, following dimensionless parameters can be considered.

$$\hat{x}_1=\frac{x_1}{h}\ \ ;\ \ \hat{y}_1=\frac{y_1}{h}\ \ ;\ \ \hat{x}_2=\frac{x_2}{h}\ \ ;\ \ \hat{y}_2=\frac{y_2}{h}$$

$$\Omega t=T\ \ ;\ \ \frac{d}{dT}=\Omega\frac{d}{dT} \tag{6}$$

where h is the radial clearance between the disk and the stator, t is time variable, and Ω is rotational speed of the shaft. Now the dimensionless governing equations of motion can be written as follows:

$$\hat{\ddot{x}}_1+\frac{c_1}{m_1\Omega}\hat{\dot{x}}_1+\frac{k}{m_1\Omega^2}\left(\hat{x}_1-\hat{x}_2\right)= \Delta\cdot\frac{F_x\left(\hat{x}_1,\hat{y}_1\right)}{m_1\Omega^2h}+\frac{e_m}{h}\cos\left(T\right)+\frac{kr_0}{m_1\Omega^2h}\cos\left(T-\beta\right)$$

$$\hat{\ddot{y}}_1+\frac{c_1}{m_1\Omega}\hat{\dot{y}}_1+\frac{k}{m_1\Omega^2}\left(\hat{y}_1-\hat{y}_2\right)= \Delta\cdot\frac{F_y\left(\hat{x}_1,\hat{y}_1\right)}{m_1\Omega^2h}+\frac{e_m}{h}\sin\left(T\right) +\frac{kr_0}{m_1\Omega^2h}\ \sin\left(T-\beta\right)-\frac{g}{\Omega^2h} \tag{7}$$

$$\hat{\ddot{x}}_2+\frac{c_2}{m_2\Omega}\hat{\dot{x}}_2+\frac{k}{2m_2\Omega^2}\left(-\hat{x}_1+\hat{x}_2\right)=\frac{p_x\left(\hat{x}_2,\hat{y}_2\right)}{m_2\Omega^2h}$$

$$\hat{\ddot{y}}_2+\frac{c_2}{m_2\Omega}\hat{\dot{y}}_2+\frac{k}{2m_2\Omega^2}\left(-\hat{y}_1+\hat{y}_2\right)=\frac{p_y\left(\hat{x}_2,\hat{y}_2\right)}{m_2\Omega^2h}-\frac{g}{\Omega^2h}$$

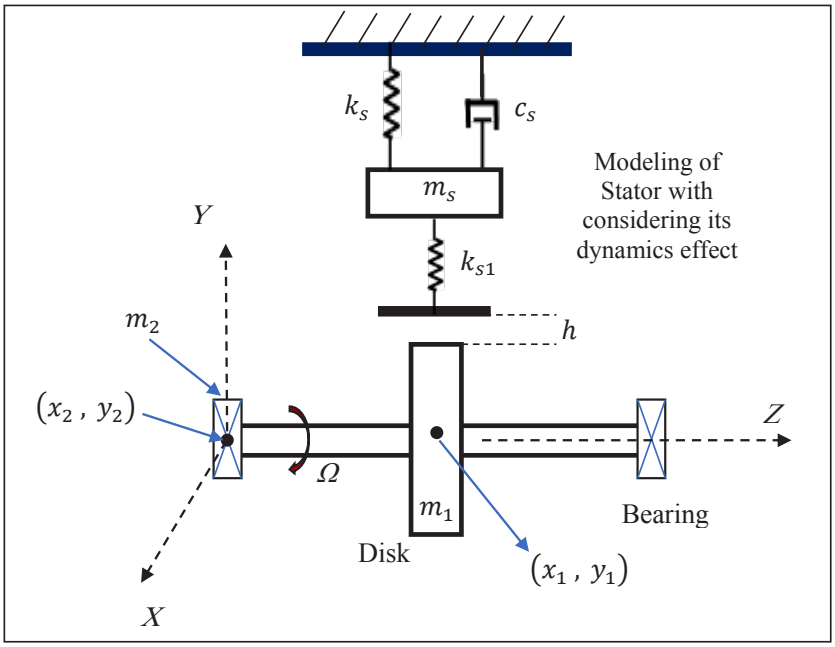

Fig. 3. Schematic model of a rotor-disk-bearing-stator system with considering stator dynamics effect

2- 2- Modeling of the system with considering the stator dynamics

In this section, the effect of stator dynamics is also considered in the mathematical modeling of the system under rub-impact between disk and stator. A schematic of rotor-disk-bearing-stator system modeling with considering the stator dynamics effect has been shown in Fig. 3. In this case, the stator is modeled with a mass m_s , a linear spring K_s , and a damper c_s as shown in Fig. 3.

According to the previous section, by using Jeffcott model, governing equations of motion of the system under rub-impact with considering the effect of stator dynamics can be derived as follows:

$$m_1\ddot{x}_1+c_1\dot{x}_1+k\left(x_1-x_2\right)=\Delta\cdot F_x\left(x_1,y_1\right)+m_1e_m\Omega^2\cos\left(\Omega t\right)+kr_0\cos\left(\Omega t-\beta\right)$$

$$m_1\ddot{y}_1+c_1\dot{y}_1+k\left(y_1-y_2\right)=\Delta\cdot F_y\left(x_1,y_1\right)+m_1e_m\Omega^2\sin\left(\Omega t\right)+kr_0\sin\left(\Omega t-\beta\right)-m_1g$$

$$m_2\ddot{x}_2+c_2\dot{x}_2+\frac{k}{2}\left(-x_1+x_2\right)=p_x\left(x_2,y_2\right) \tag{8}$$

$$m_2\ddot{y}_2+c_2\dot{y}_2+\frac{k}{2}\left(-y_1+y_2\right)=p_y\left(x_2,y_2\right)-m_2g$$

$$m_s\ddot{x}_s+c_s\dot{x}_s+k_sx_s=-\Delta\cdot F_x\left(x_1,y_1\right)$$

$$m_s\ddot{y}_s+c_s\dot{y}_s+k_sy_s=-\Delta\cdot F_y\left(x_1,y_1\right)-m_sg$$

$$\Delta=\begin{cases}0 & if \quad \tilde{r}\le h\\ 1 & if \quad \tilde{r}>h\end{cases}$$

$$F_x=-F_N\cos\left(\phi\right)+F_t\sin\left(\phi\right)=-k_{s1}\left(1-\frac{h}{\tilde{r}}\right)\left[\left(x_1-x_s\right)-f\left(y_1-y_s\right)\right] \tag{9}$$

$$F_y=-F_N\sin\left(\phi\right)-F_t\cos\left(\phi\right)=-k_{s1}\left(1-\frac{h}{\tilde{r}}\right)\left[f\left(x_1-x_s\right)+\left(y_1-y_s\right)\right]$$

$$\tilde{r}=\sqrt{\left(x_1-x_s\right)^2+\left(y_1-y_s\right)^2}$$

where $p_x\left(x_2,y_2\right)$, and $p_y\left(x_2,y_2\right)$ are oil film nonlinear forces, β is the angle between unbalance and the bending, $F_x\left(x_1,y_1\right)$ and $F_y\left(x_1,y_1\right)$ are rubbing forces between the disk and the stator, c_1 and c_2 are damping coefficients of the rotating shaft and journal bearing, m_1 and m_2 are mass of the disk and lumped mass of the journal bearing, g is acceleration of gravity, and f is the coefficient of friction between the disk and the stator in rub-impact.

Again, by using the following dimensionless parameters

$$\hat{x}_1=\frac{x_1}{h}\ ;\ \hat{y}_1=\frac{y_1}{h}\ ;\ \hat{x}_2=\frac{x_2}{h}\ ;\ \hat{y}_2=\frac{y_2}{h}$$

$$\hat{x}_s=\frac{x_s}{h}\ ;\ \hat{y}_s=\frac{y_s}{h} \tag{10}$$

$$\Omega t=T\ ;\ \frac{d}{dT}=\Omega\frac{d}{dT}$$

$$\tilde{r}=\sqrt{\left(x_1-x_s\right)^2+\left(y_1-y_s\right)^2}$$

The Eq. (8) can be rewritten as dimensionless form as follows:

$$\hat{x}_1''+\frac{c_1}{m_1\Omega}\hat{x}_1'+\frac{k}{m_1\Omega^2}\left(\hat{x}_1-\hat{x}_2\right)=\Delta\cdot\frac{F_x\left(\hat{x}_1,\hat{y}_1\right)}{m_1\Omega^2h}+\frac{e_m}{h}\cos\left(T\right)+\frac{kr_0}{m_1\Omega^2h}\cos\left(T-\beta\right)$$

$$\hat{y}_1''+\frac{c_1}{m_1\Omega}\hat{y}_1'+\frac{k}{m_1\Omega^2}\left(\hat{y}_1-\hat{y}_2\right)=\Delta\cdot\frac{F_y\left(\hat{x}_1,\hat{y}_1\right)}{m_1\Omega^2h}+\frac{e_m}{h}\sin\left(T\right)+\frac{kr_0}{m_1\Omega^2h}\sin\left(T-\beta\right)-\frac{g}{\Omega^2h}$$

$$\hat{x}_2''+\frac{c_2}{m_2\Omega}\hat{x}_2'+\frac{k}{2m_2\Omega^2}\left(-\hat{x}_1+\hat{x}_2\right)=\frac{p_x\left(\hat{x}_2,\hat{y}_2\right)}{m_2\Omega^2h} \tag{11}$$

$$\hat{y}_2''+\frac{c_2}{m_2\Omega}\hat{y}_2'+\frac{k}{2m_2\Omega^2}\left(-\hat{y}_1+\hat{y}_2\right)=\frac{p_y\left(\hat{x}_2,\hat{y}_2\right)}{m_2\Omega^2h}-\frac{g}{\Omega^2h}$$

$$\hat{x}_s''+\frac{c_s}{m_s\Omega}\hat{x}_s'+\frac{k_s}{m_s\Omega^2}\hat{x}_s=-\Delta\cdot\frac{F_x\left(\hat{x}_1,\hat{y}_1\right)}{m_s\Omega^2h}$$

$$\hat{y}_s''+\frac{c_s}{m_s\Omega}\hat{y}_s'+\frac{k_s}{m_s\Omega^2}\hat{y}_s=-\Delta\cdot\frac{F_y\left(\hat{x}_1,\hat{y}_1\right)}{m_s\Omega^2h}-\frac{g}{\Omega^2h}$$

3- Numerical Simulation and Analysis of Results

3- 1- Numerical results of the system behavior without considering the stator dynamics

In the numerical solution, the fourth order Runge-Kutta method with variable time step is applied to solve the governing equations of the system with Eqs. (7) and (11). Rotational speed ($s=\Omega$) has been selected as a control parameter. The analysis is done both with and without considering the dynamics of the stator. To identify system behavior, special tools related to this phenomenon such as time history, phase plane diagram, power spectrum, Poincaré maps, bifurcation diagram, and maximum Lyapunov exponent are used. The numerical parameters in the Table 1 are used to analyze of dynamic behavior of the system without considering stator dynamics.

By numerical solution of Eq. (6), the displacement bifurcation diagram of $\hat{x}_1$ versus rotating shaft is depicted in Figs. 4 and 5. The results from Figs. 4 and 5 show that the system motion at speed $\Omega=100$ to $\Omega=226.5$ rad/s is first order periodic. Then at speed $\Omega=226.6$ rad/s, rub-impact between disk stator happens, and motion goes to a sub-harmonic mood with a period (2T). Moving at a speed of 253.4 to 279 rad/s, the system turns back to the first order state periodic. This behavior is also shown in Fig. 6 at speeds 255 rad/s. This claim is proved by time series, phase plane, power spectrum diagrams, and Poincaré maps that are diagnostic tools to identify system behavior.

Table 1. Rotor-bearing system numerical parameters

Parameter	Data	unit
m_1	32	kg
m_2	4	kg
c_1	2100	N.s/m
c_2	1050	N.s/m
k	2.5×10^4	N/m
k_{s1}	7.5×10^6	N/m
r_0	0.02	mm
β	$\pi/4$	-
e_m	0.05	mm
h	0.11	mm
g	9.8	N/kg
f	0.1	-

At speed range of 280 to 313.3 rad/s, the system enters third-order sub-harmonic motion. The motion in the range of speed 313.4 to 320 rad/s is a first order periodic. The motion behavior of the system changes to third order motion (3T) when the speed goes up to 320.1 rad/s and this continues up to 325 rad/s. The system has a chaotic behavior of motion at the speed range of $325<\Omega<334$ rad/s, and at $335<\Omega<345$ rad/s, the motion of the system has quasi-periodic behavior. The system has chaotic behavior at a speed range of 345 to 455 rad/s, also. According to the time series diagram, plane phase diagram, Poincare maps, power spectrum, it is well known at speed 361 rad/s. At speed range of 456 to 475 rad/s, the system enters fourth-order periodic motion (4T) and then at range 476 to 609 rad/s enters the chaotic motion and again at speed range, 642.8 to 609.2 rad/s, returns to second order periodic motion (2T). At $643<\Omega<730$ rad/s the system has a chaotic motion and from $\Omega=731$ up to $\Omega=770.6$ rad/s enters to periodically motion (2T). Finally, the system has periodically motion behavior at the speed range 770.7 to 811 rad/s. At speed 836.6 to 909 rad/s, the system has motion behavior between quasi-periodic and chaotic. At speed 910 rad/s, it enters the periodic motion (4T), and this continues up to 929 rad/s. At the range $930<\Omega<1000$ rad/s, the system has a periodic motion (2T). Fig. 5 shows the system bifurcation diagram at the range of $1000<\Omega<2500$ rad/s. According to Fig. 5 and what mentioned above, it can be said that at the range $1000<\Omega<1917$ rad/s and at the range $1917<\Omega<2110$ rad/s, the system has periodic behavior and chaotic behavior, respectively. Again in the range $2110<\Omega<2500$ rad/s, the motion of the system is periodic.

The above-mentioned behavior of the system at the range $280<\Omega<2500$ rad/s can be proved by Figs. 7 to 11 that are diagnostic tools to identify system behavior. Time series

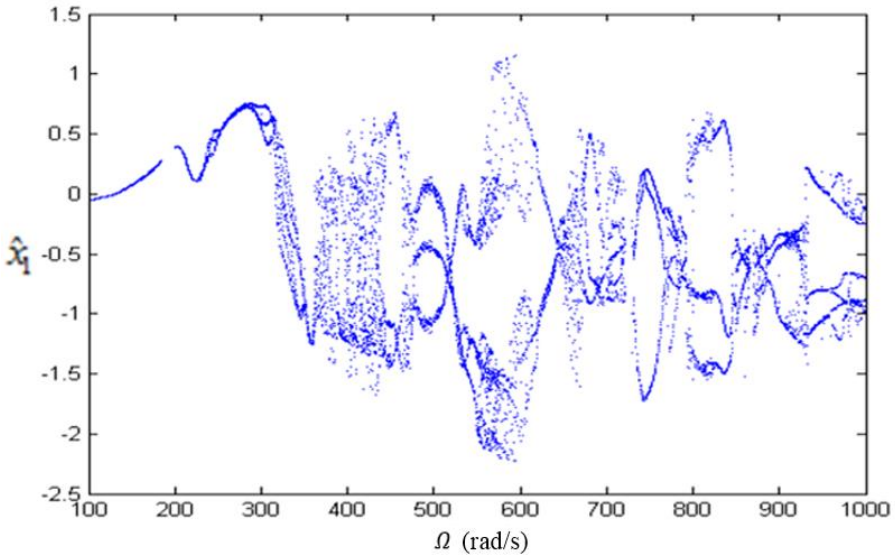

Fig. 4. Bifurcation diagram of the rotor-bearing system with the initial deflection, considering nonlinear oil film pressure

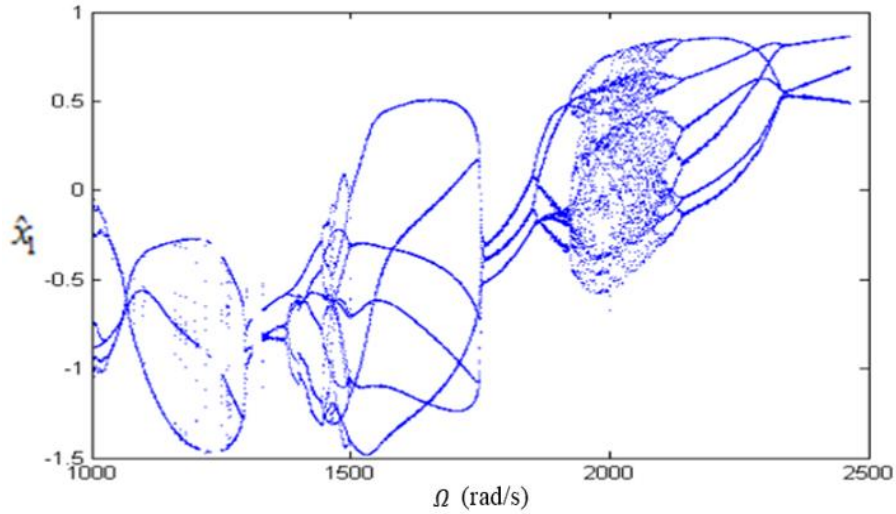

Fig. 5. Bifurcation diagram of the rotor-bearing system with the initial deflection, considering nonlinear oil film pressure (continued)

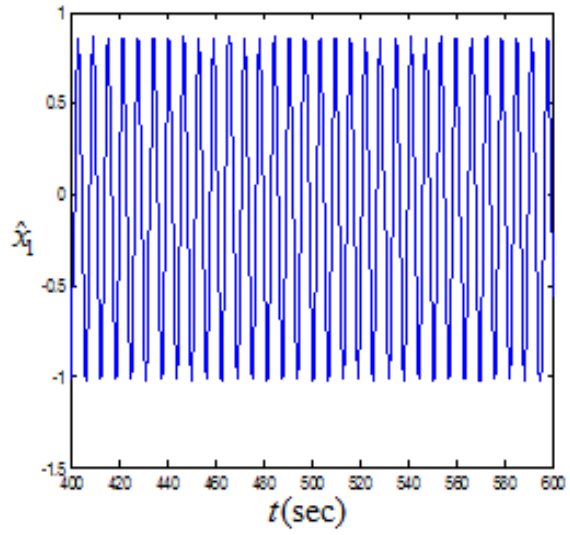

A) Time series

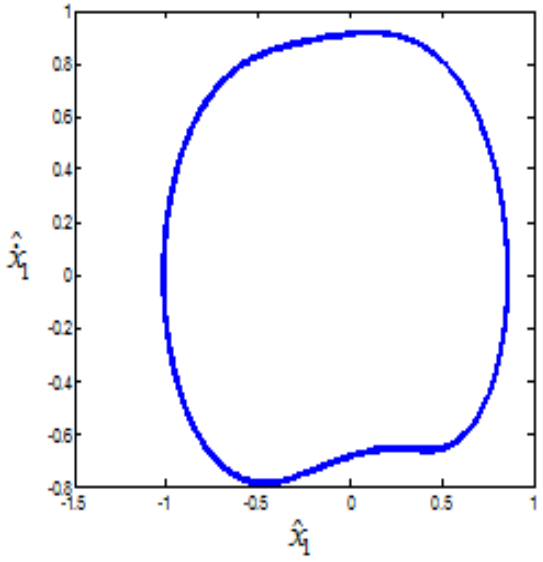

B) Phase plane graph

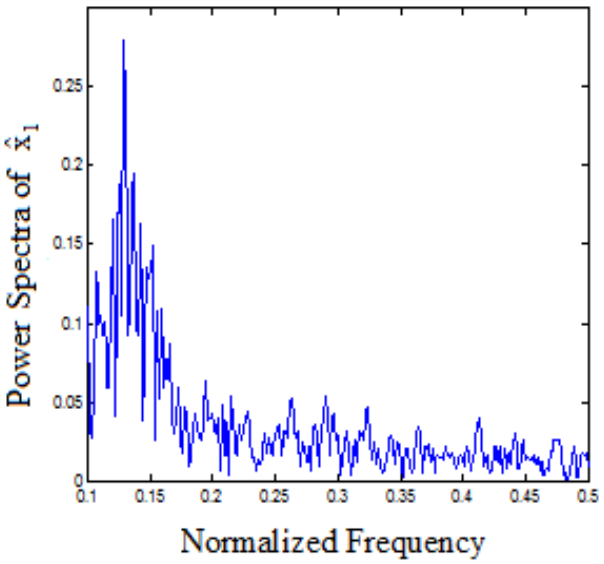

C) Power spectrum

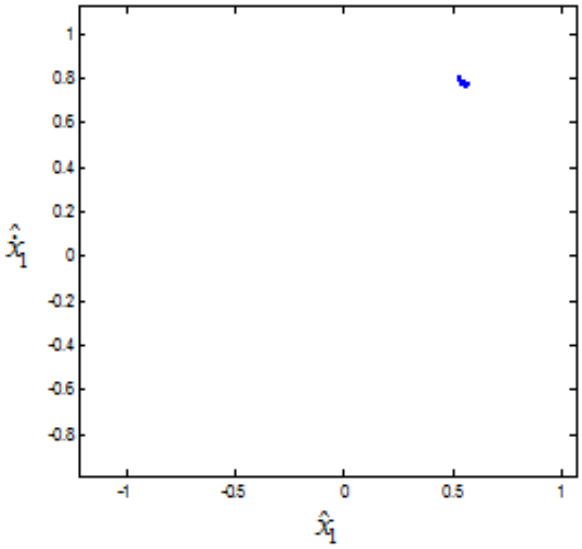

D) Poincaré map

Fig. 6. Time series, Phase plane graph, Power spectrum, and Poincaré map at Ω=255 rad/s

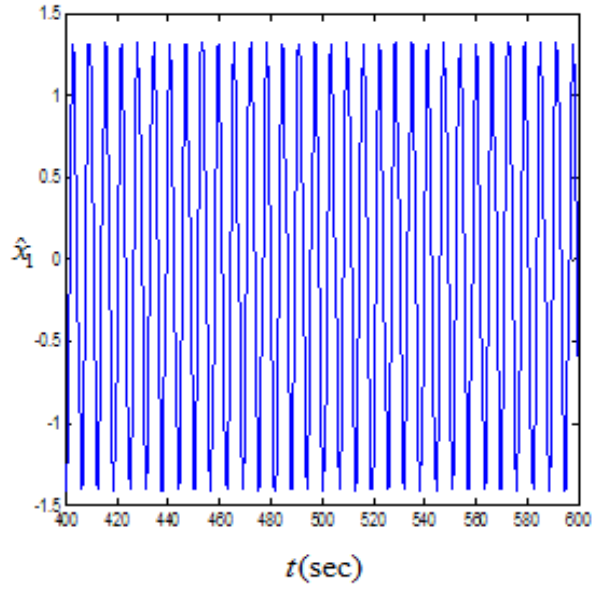

A) Time series

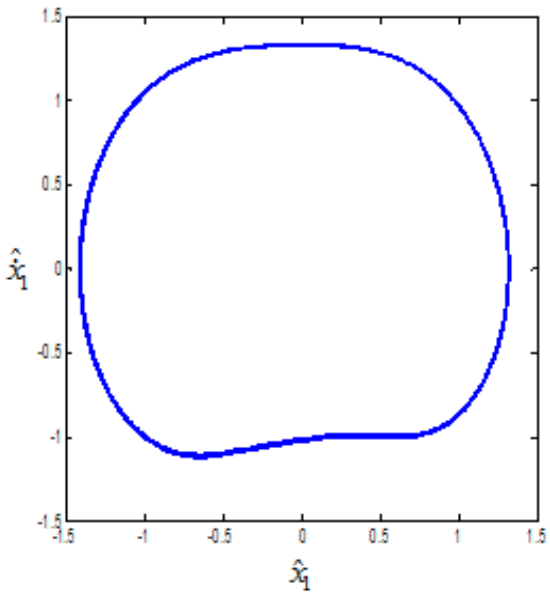

B) Phase plane graph

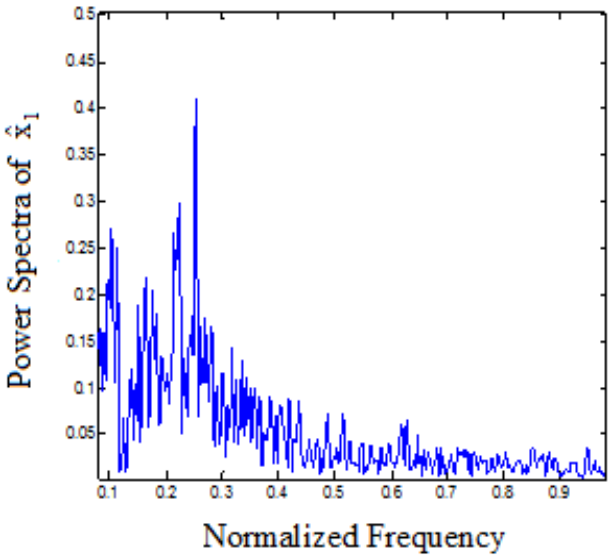

C) Power spectrum

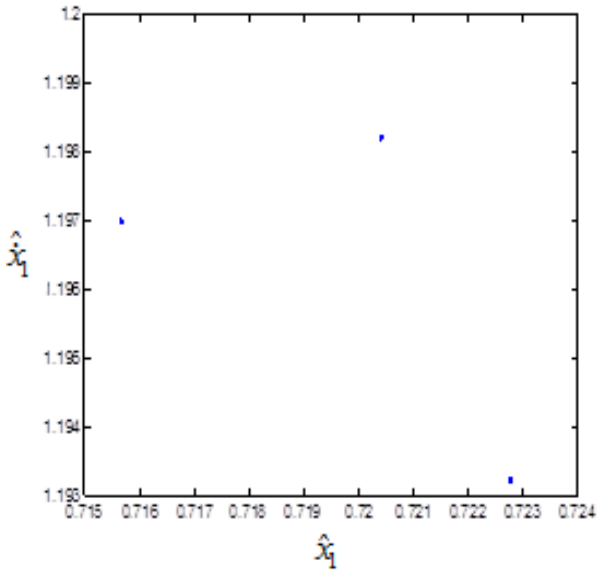

D) Poincaré map

Fig. 7. Time series, Phase plane graph, Power spectrum, and Poincaré map at Ω=280 rad/s

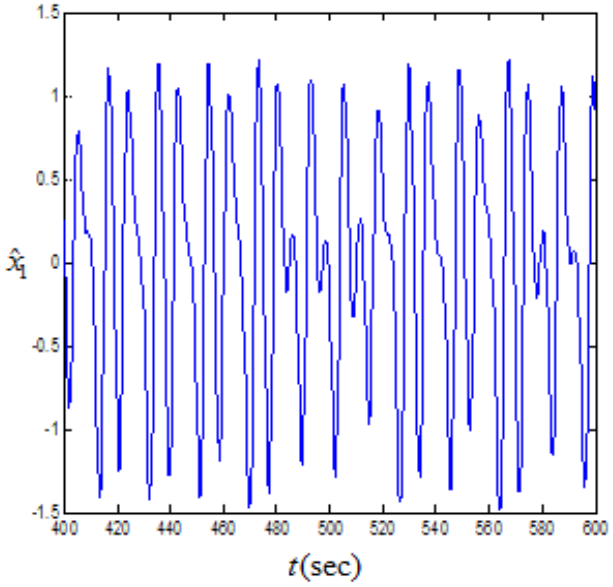

A) Time series

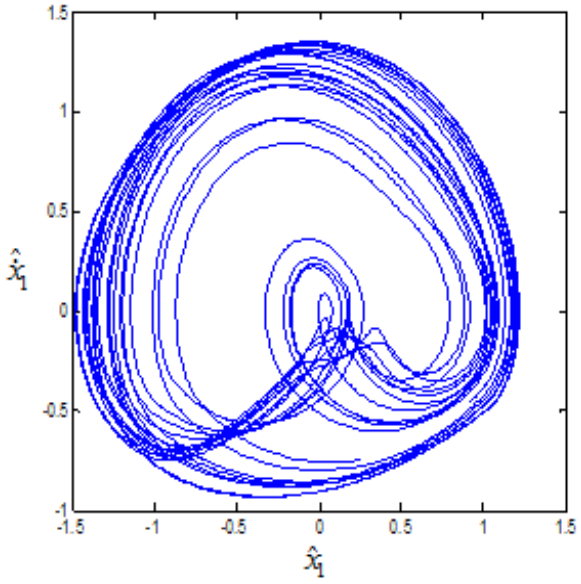

B) Phase plane graph

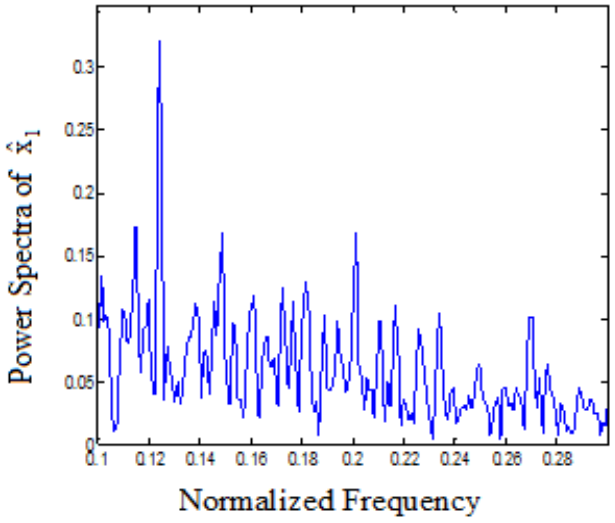

C) Power spectrum

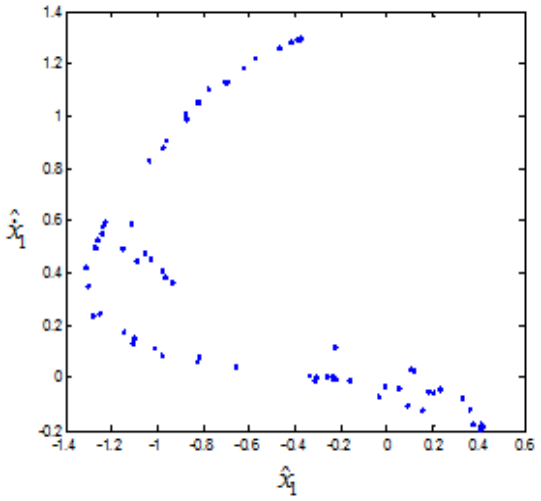

D) Poincaré map

Fig. 8. Time series, Phase plane graph, Power spectrum, and Poincaré map at Ω=361 rad/s

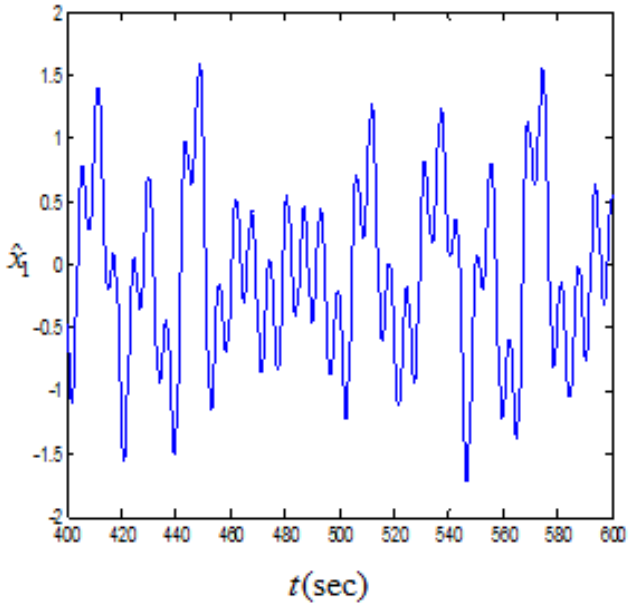

A) Time series

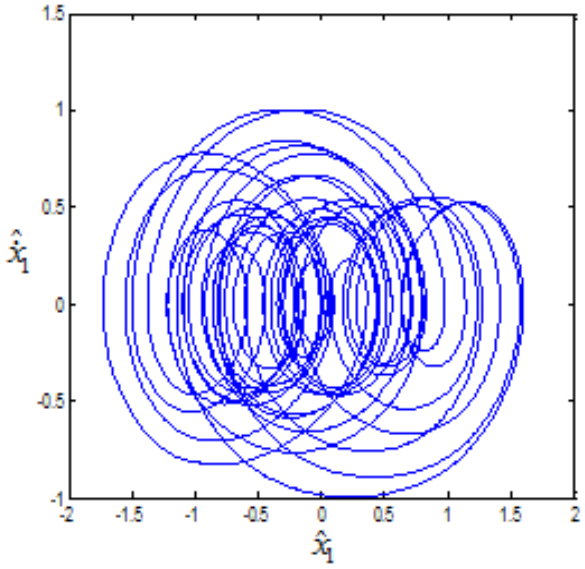

B) Phase plane graph

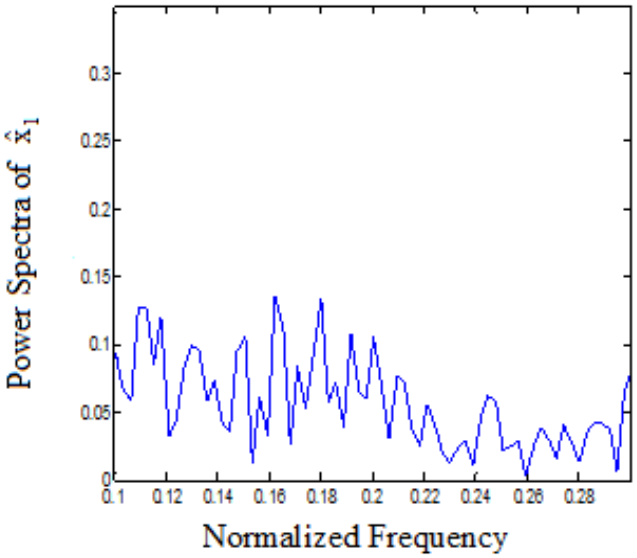

C) Power spectrum

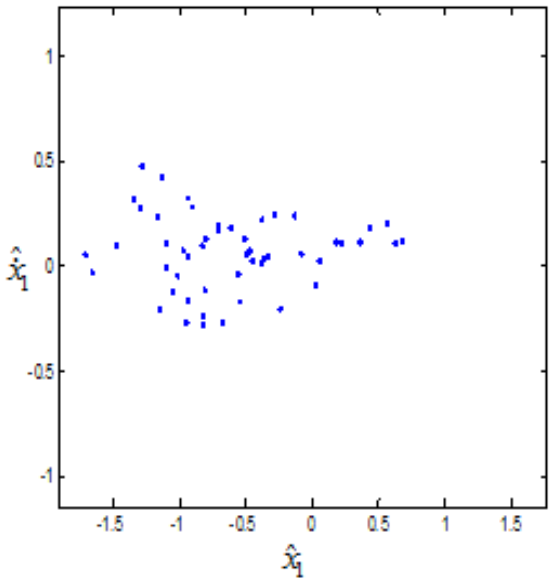

D) Poincaré map

Fig. 9. Time series, Phase plane graph, Power spectrum, and Poincaré map at Ω=700 rad/s

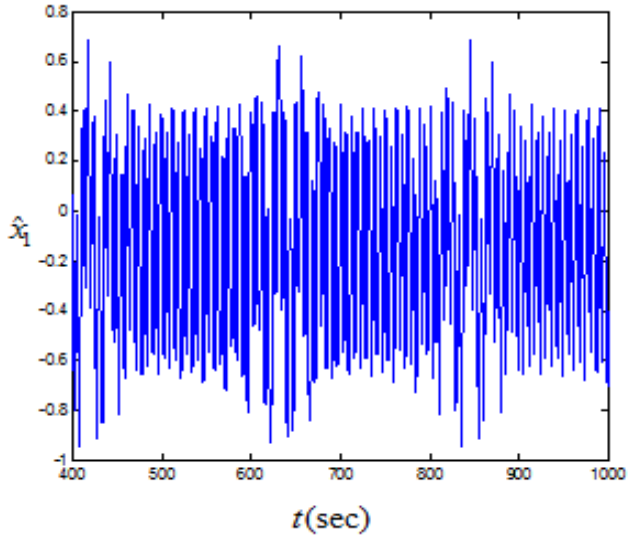

A) Time series

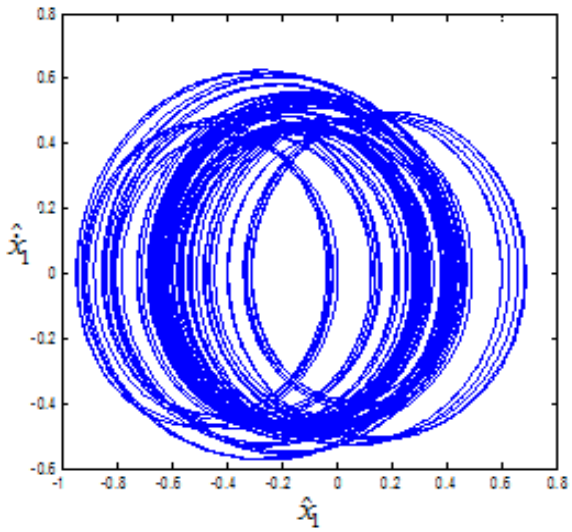

B) Phase plane graph

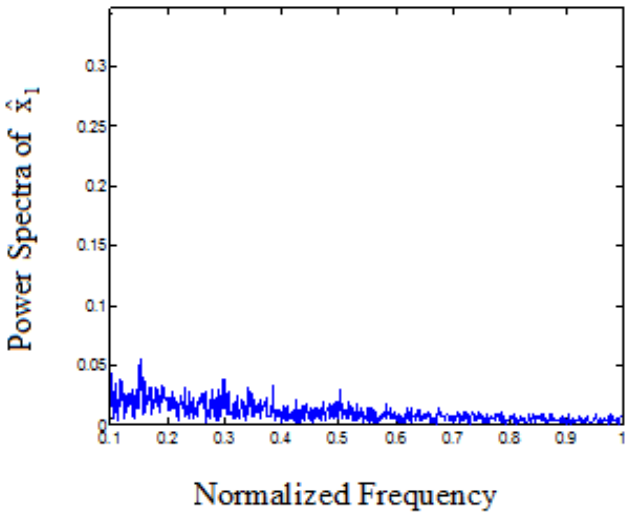

C) Power spectrum

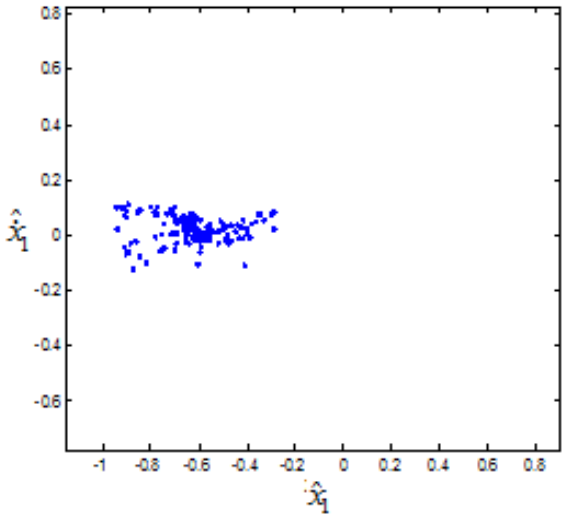

D) Poincaré map

Fig. 10. Time series, Phase plane graph, Power spectrum, and Poincaré map at Ω=900 rad/s

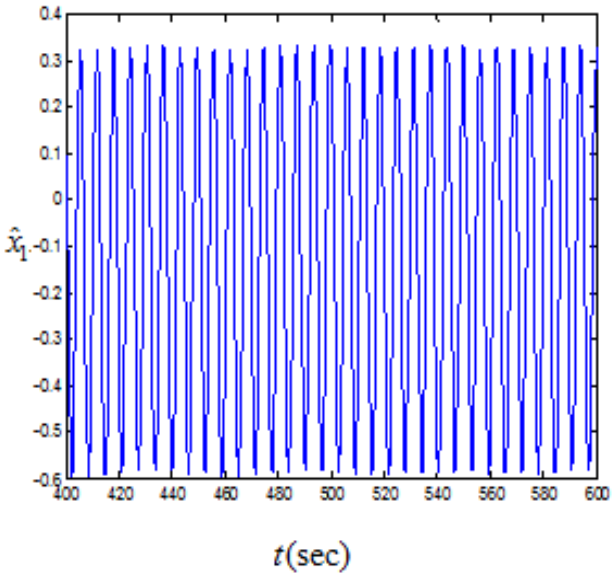

A) Time series

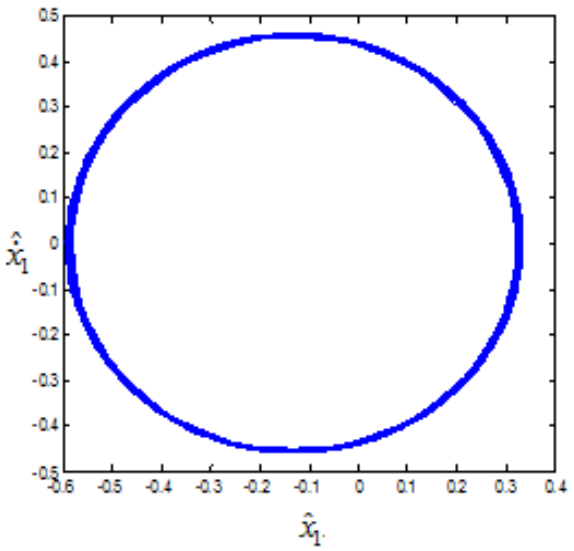

B) Phase plane graph

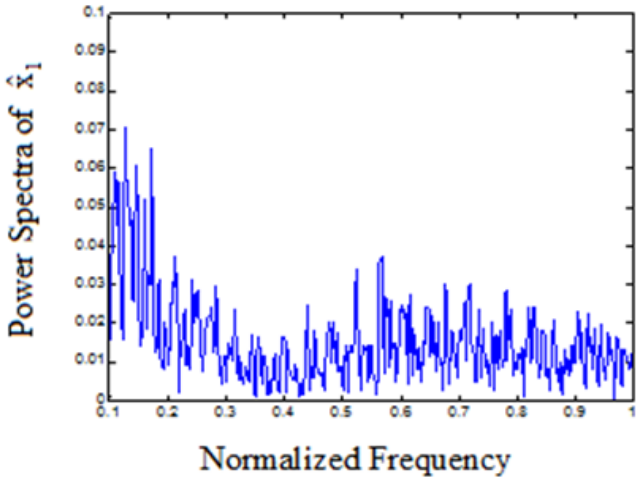

C) Power spectrum

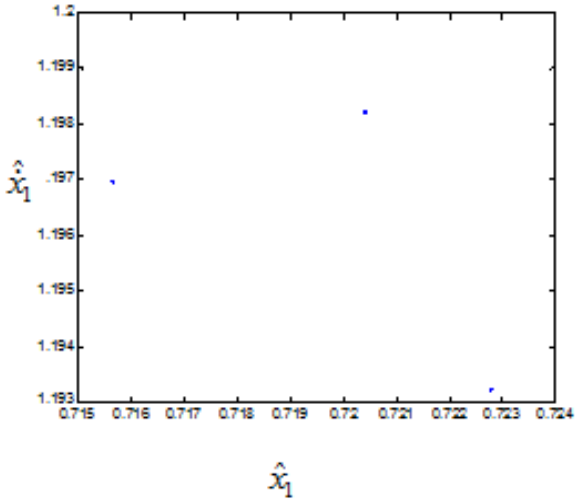

D) Poincaré map

Fig. 11. Time series, Phase plane graph, Power spectrum, and Poincaré map at Ω=2400 rad/s

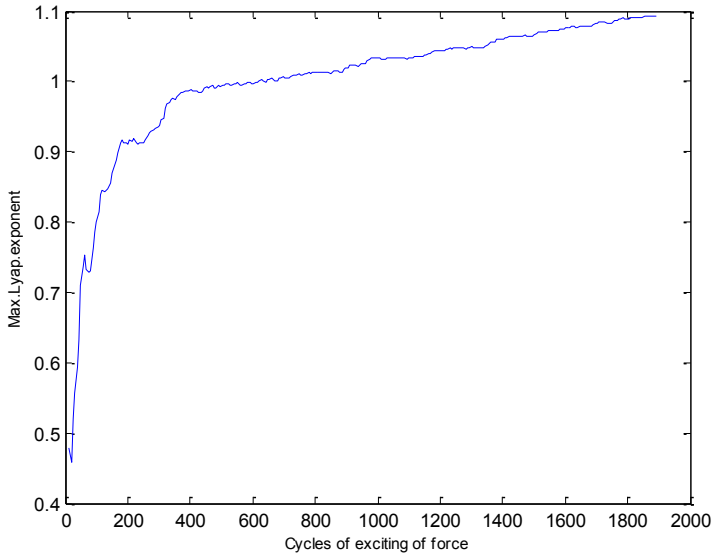

Fig. 12. Maximum Lyapunov exponent at speed Ω=361 rad/s

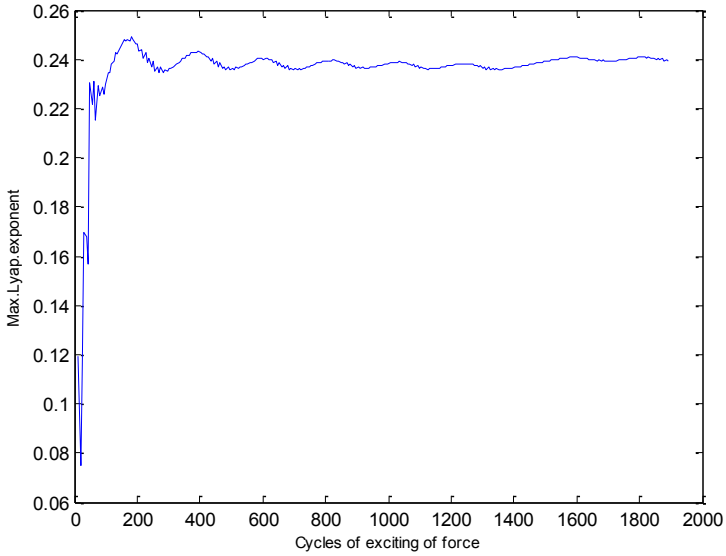

Fig. 13. Maximum Lyapunov exponent at speed Ω=900 rad/s

diagrams, phase plane graphs, power spectrum diagrams, and Poincaré maps at rotational speeds 280 rad/s, 361 rad/s, 700 rad/s, 900 rad/s, and 2400 rad/s have been presented in Figs. 7 to 11, respectively.

The analysis of the system motion behavior has been benefited from the bifurcation diagrams, methods of system behavior identification, including time-series, phase plane diagram, power spectrum diagrams, and Poincaré maps at different rotational speeds. But at some speeds, motion type detection of the system from the time-series and power spectrum is difficult. On the other hand, when identifying sub-harmonic motion having a higher period than quasi-periodic motion, it is likely to make a mistake. Consequently, it is suggested to use another system behavior identification tools which are more exact than the others. One of the most powerful methods of chaotic motion detection is the use of the maximum Lyapunov exponent.

At rotational speeds, 361 and 900 rad/s, time series diagram, phase plane, power spectrum, and Poincaré maps are depicted. Using the maximum Lyapunov exponent, the claims are investigated. According to the diagrams depicted at $\Omega = 361$ rad/s, the initial diagnosis results in chaotic motion. Using the Maximum Lyapunov Exponent in Fig. 12, the validity of this claim is examined. As maximum Lyapunov exponent is positive, the declaration about chaotic motion at this speed is confirmed. Also, at $\Omega = 900$ rad/s, according to the diagrams, it is difficult to identify motion behavior. For this purpose, we use the maximum Lyapunov exponent which depicted in Fig. 13. Fig. 13 shows that the motion behavior of the system is chaotic at this speed.

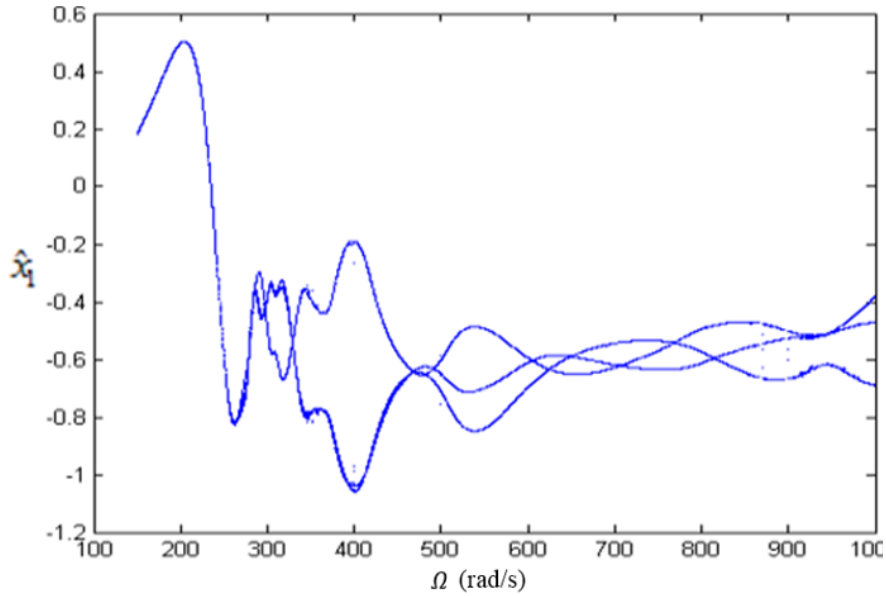

Fig. 14. Bifurcation diagram of the rotor-bearing-stator system with the initial deflection, taking into account nonlinear oil film pressure

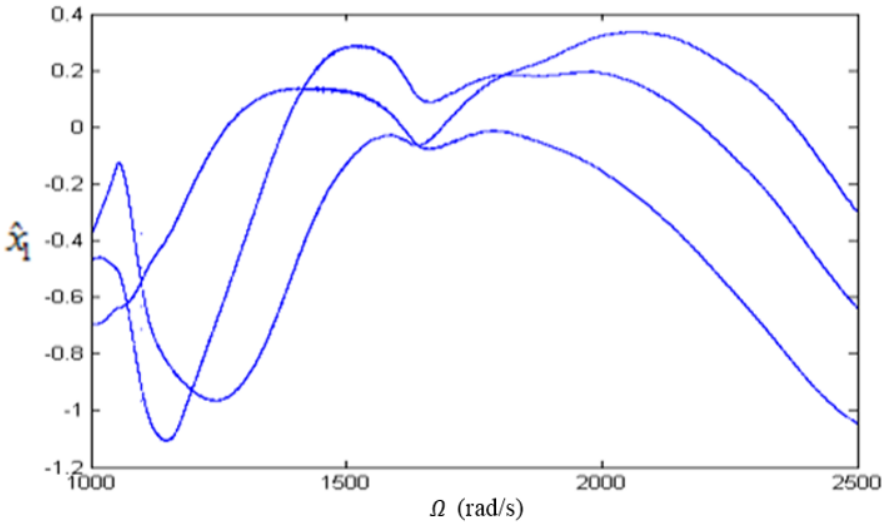

Fig. 15. Bifurcation diagram of the rotor-bearing-stator system with the initial deflection, taking into account nonlinear oil film pressure (continued)

3- 2- Numerical results of the system behavior with considering the stator dynamics

To investigate the motion behavior of the system with considering the stator dynamics effect, numerical data of Table 2 is used. Figs. 14 and 15 show the bifurcation diagrams of the system in the y-direction.

The Figs. 14 and 15 show at the speed range 150< Ω <2500 rad/s, the system has a periodic and regular behavior. While in Figs. 4 and 5 the absence of stator dynamics effect and only considering the force rubbing depicted at speed range 150< Ω <900 rad/s, non-periodic and chaotic behavior at some speed were shown. To analyze Figs. 14 and 15 tools including time series, phase plane, power spectrum, and Poincare map are applied. At speeds between 150< Ω <330 rad/s regular and periodic behavior is (1T).

The system has a regular periodic motion (2T) at the range of 331< Ω <467 rad/s. Once again at speed range 467< Ω <1099 rad/s, it goes into periodic motion (3T). At Ω =1100 rad/s, the system motion is quasi-periodic. Then the quasi-periodic motion goes up to Ω =1449 rad/s. The system enters a regular and periodic motion behavior (5T) at range Ω =1450 rad/s to Ω =1480 rad/s. The system at Ω =1481 rad/s enters the periodic motion (3T) and this behavior continues up to Ω =2500 rad/s.

The above behaviors of the system are also proved by time series diagrams, phase plane graphs, power spectrum diagrams, and Poincaré maps at rotational speeds in Figs. 16 to 18 at rotational speeds 170 rad/s, 1100 rad/s, and 1450 rad/s, respectively.

Table 2. The numerical parameters of the rotor-disk-bearing-stator system by considering the stator dynamics effect

Parameter	Data	unit
m_1	32	kg
m_2	4	kg
m_s	10	kg
c_1	2100	N.s/m
c_2	1050	N.s/m
c_s	2100	N.s/m
k	2.5×10^4	N/m
k_{s1}	7.5×10^6	N/m
k_s	7.5×10^6	N/m
h	0.11	mm
g	9.8	N/kg
f	0.1	-
r_0	0.02	mm
β	$\pi/4$	-
e_m	0.05	mm
h	0.11	mm

4- Validation

The governing Eqs. (8) and (9) were derived for the rotor-disk-bearing system assuming rub-impact with considering the effect of the stator dynamics. In a special case, for $k_S \to \infty$ and so $x_S \approx 0$, the governing Eqs. (8) and (9) are simplified as Eqs. (1) to (5) for the rotor-disk-bearing system under rub-impact without considering the effect of the stator dynamics. It should be noted that the Eqs. (1) to (5) are suitably compatible with the ones presented in References [7,17].

Furthermore, for $k_S = 7.5 \times 10^{10}$ (rigid case of the mass m_S or without considering the stator dynamics), the results for numerical simulation of the displacement bifurcation diagram of $\hat{x}_1$ according to variation of shaft rotating speed is presented in Fig. 19. From comparing Figs. 19 and 4, it is seen that they are in good agreement with each other.

5- Conclusion

In the present article, the effect of the stator dynamics on motion behavior of the rotor-disk-bearing system was studied. Bifurcation diagrams of both systems with/without considering the stator dynamics were depicted, and were analyzed at different speeds. Finally, we concluded that disregarding the stator dynamics effect could cause the system to have a chaotic motion behavior. While considering the stator dynamics and using suitable numerical parameters, we could remove the chaotic motion behavior of the system. In this way, the system would have periodic and regular motion in a wide range of speeds. The results show that modeling of the stator dynamics has a significant impact on the predicted response of the rotor-disk-bearing system with rub-impact between disk and stator. These results can be also significant to control the chaotic motion behavior of the system for design engineers.

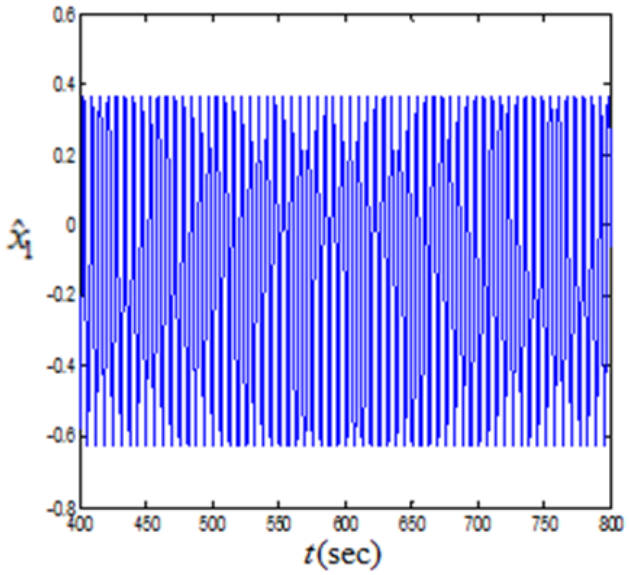

A) Time series

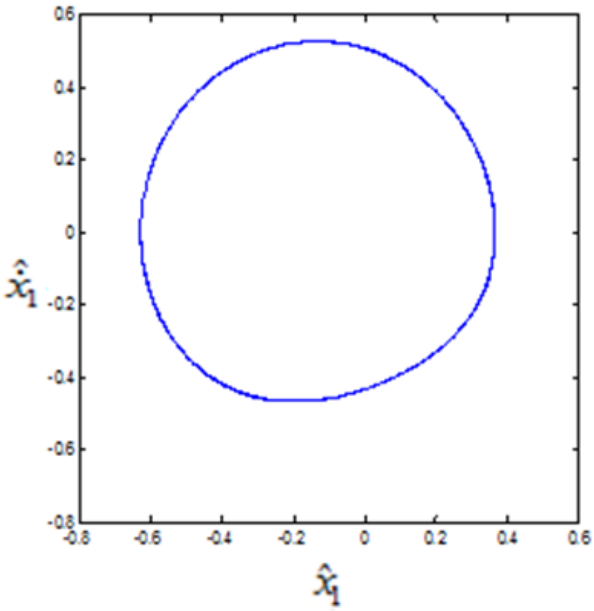

B) Phase plane graph

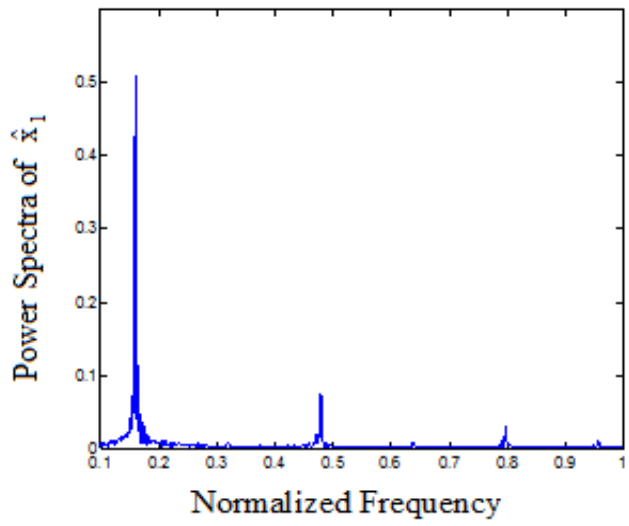

C) Power spectrum

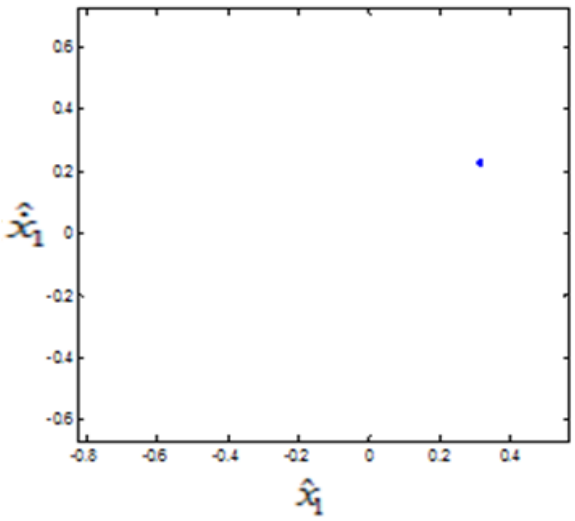

D) Poincaré map

Fig. 16. Time series, Phase plane graph, Power spectrum, and Poincaré map at Ω=170 rad/s

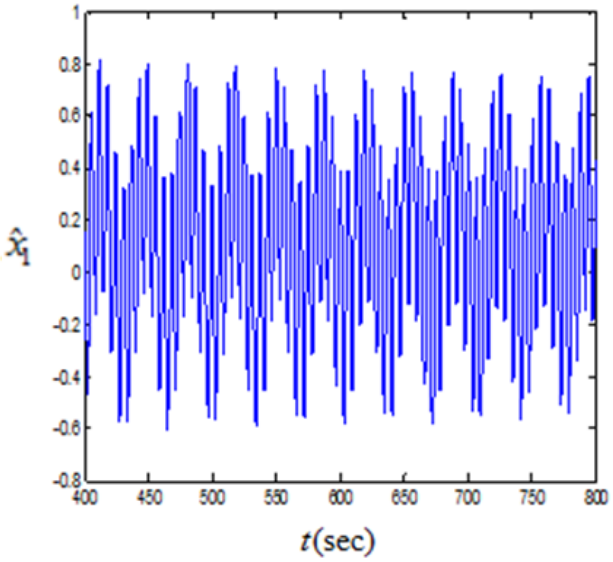

A) Time series

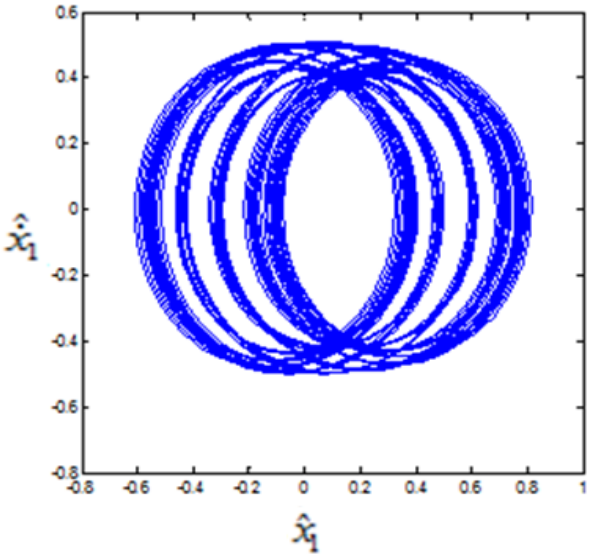

B) Phase plane graph

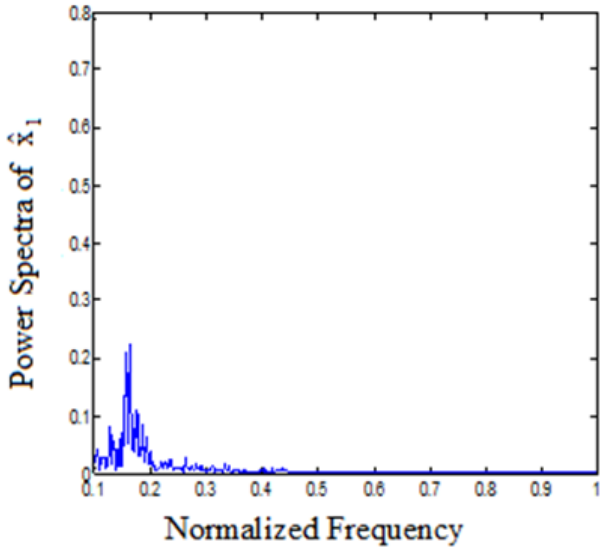

C) Power spectrum

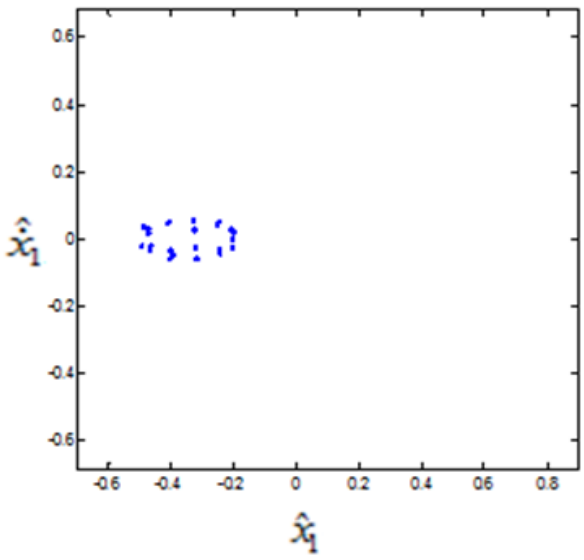

D) Poincaré map

Fig. 17. Time series, Phase plane graph, Power spectrum and, and Poincaré map at Ω=1100 rad/s

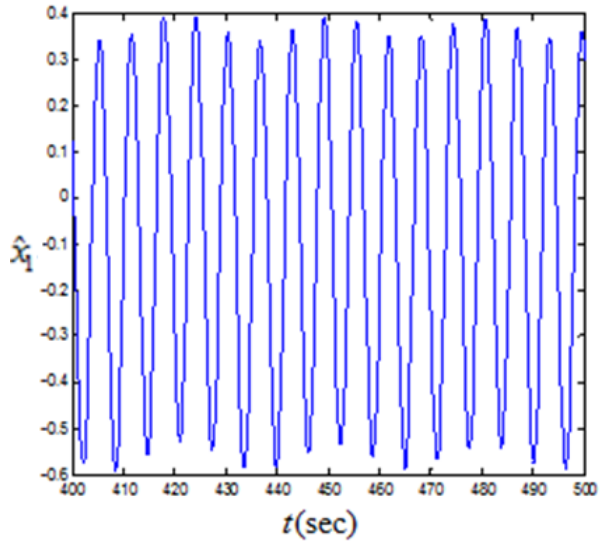

A) Time series

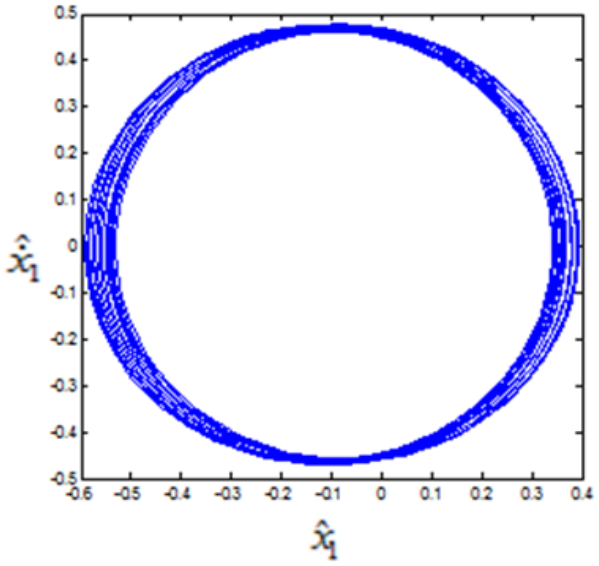

B) Phase plane graph

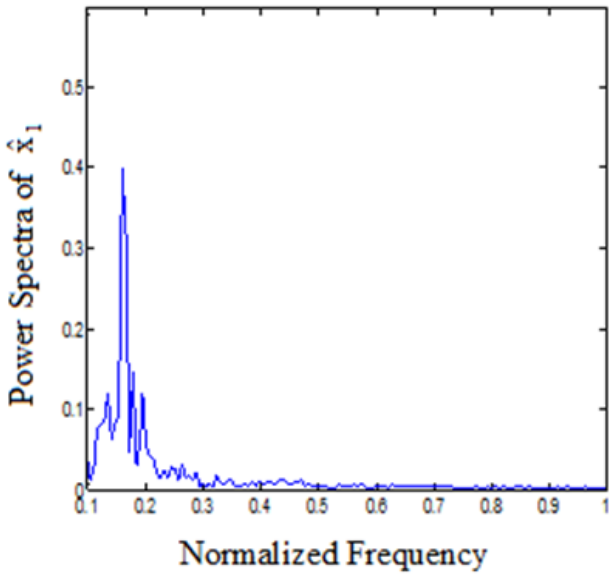

C) Power spectrum

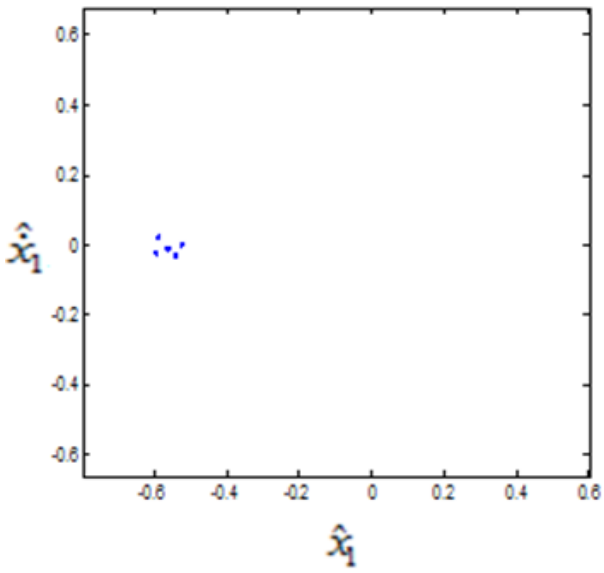

D) Poincaré map

Fig. 18. Time series, Phase plane graph, Power spectrum, and Poincaré map at Ω=1450 rad/s

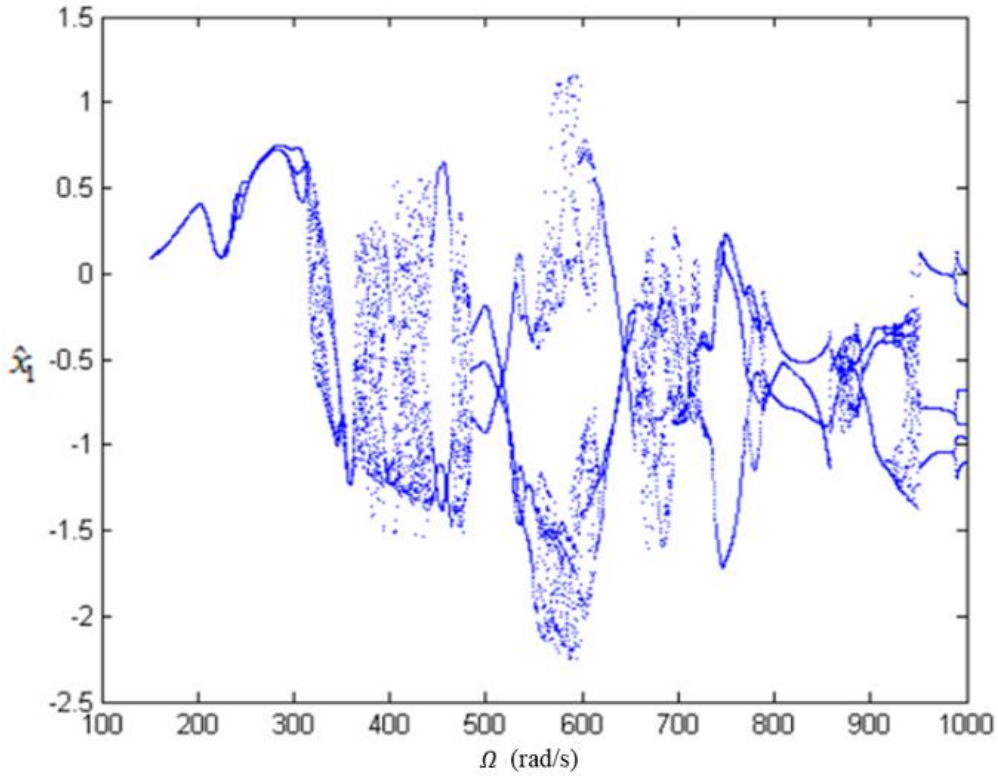

Fig. 19. Bifurcation diagram of the rotor-disk-bearing-stator system with considering the effect of stator dynamics for k_S=7.5×10^{10} N/m

References

[1] A. Muszynska, Rotordynamics, CRC press, 2005.

[2] H. Khanlo, M. Ghayour, S. Ziaei-Rad, Chaotic vibration analysis of rotating, flexible, continuous shaft-disk system with a rub-impact between the disk and the stator, Communications in Nonlinear Science and Numerical Simulation, 16(1) (2011) 566-582.

[3] H. Khanlo, M. Ghayour, S. Ziaei-Rad, The effects of lateral–torsional coupling on the nonlinear dynamic behavior of a rotating continuous flexible shaft–disk system with rub–impact, Communications in Nonlinear Science and Numerical Simulation, 18(6) (2013) 1524-1538.

[4] Y.S. Choi, On the contact of partial rotor rub with experimental observations, KSME international journal, 15(12) (2001) 1630-1638.

[5] F. Chu, W. Lu, Stiffening effect of the rotor during the rotor-to-stator rub in a rotating machine, Journal of Sound and vibration, 308(3-5) (2007) 758-766.

[6] X. Shen, J. Jia, M. Zhao, Nonlinear analysis of a rub-impact rotor-bearing system with initial permanent rotor bow, Archive of Applied Mechanics, 78(3) (2008) 225-240.

[7] L. Xiang, A. Hu, L. Hou, Y. Xiong, J. Xing, Nonlinear coupled dynamics of an asymmetric double-disc rotor-bearing system under rub-impact and oil-film forces, Applied Mathematical Modelling, 40(7-8) (2016) 4505-4523.

[8] F. Choy, J. Padovan, Non-linear transient analysis of rotor-casing rub events, Journal of Sound and Vibration, 113(3) (1987) 529-545.

[9] A.R. Bartha, Dry friction backward whirl of rotors, ETH Zurich, 2000.

[10] W.M. Zhang, G. Meng, Stability, bifurcation and chaos of a high-speed rub-impact rotor system in MEMS, Sensors and Actuators A: Physical, 127(1) (2006) 163-178.

[11] S. Roques, M. Legrand, P. Cartraud, C. Stoisser, C. Pierre, Modeling of a rotor speed transient response with radial rubbing, Journal of Sound and Vibration, 329(5) (2010) 527-546.

[12] J. Yu, P. Goldman, D. Bently, A. Muzynska, Rotor/seal experimental and analytical study on full annular rub, Journal of Engineering for Gas Turbines and Power, 124(2) (2002) 340-350.

[13] E.E. Pavlovskaia, E. Karpenko, M. Wiercigroch, Non-linear dynamic interactions of a Jeffcott rotor with preloaded snubber ring, Journal of Sound and Vibration, 276(1-2) (2004) 361-379.

[14] Z. Feng, X.Z. Zhang, Rubbing phenomena in rotor–stator contact, Chaos, Solitons & Fractals, 14(2) (2002) 257-267.

[15] L. Hall, D. Mba, Diagnosis of continuous rotor–stator rubbing in large scale turbine units using acoustic emissions, Ultrasonics, 41(9) (2004) 765-773.

[16] H. Ma, Q. Zhao, X. Zhao, Q. Han, B. Wen, Dynamic

characteristics analysis of a rotor–stator system under different rubbing forms, Applied Mathematical Modelling, 39(8) (2015) 2392-2408.

[17] C.W. Chang-Jian, C.K. Chen, Non-linear dynamic analysis of rub-impact rotor supported by turbulent journal bearings with non-linear suspension, International Journal of Mechanical Sciences, 50(6) (2008) 1090-1113.

[18] J.D. Jeng, L. Hsu, C.-W. Hun, C.-Y. Chou, Identification for bifurcation and responses of rub-impacting rotor system, Procedia Engineering, 79 (2014) 369-377.

[19] A. Hu, L. Hou, L. Xiang, Dynamic simulation and experimental study of an asymmetric double-disk rotor-bearing system with rub-impact and oil-film instability, Nonlinear Dynamics, 84(2) (2016) 641-659.

[20] L. Xiang, X. Gao, A. Hu, Nonlinear dynamics of an asymmetric rotor-bearing system with coupling faults of crack and rub-impact under oil-film forces, Nonlinear Dynamics, 86(2) (2016) 1057-1067.

[21] L. Chen, Z. Qin, F. Chu, Dynamic characteristics of rub-impact on rotor system with cylindrical shell, International Journal of Mechanical Sciences, 133 (2017) 51-64.

[22] E. Tofighi-Niaki, P. Asgharifard-Sharabiani, H. Ahmadian, Nonlinear dynamics of a flexible rotor on tilting pad journal bearings experiencing rub–impact, Nonlinear Dynamics, 94(4) (2018) 2937-2956.

[23] K. Prabith, I.P. Krishna, A Modified Model Reduction Technique for the Dynamic Analysis of Rotor-Stator Rub, in: International Conference on Rotor Dynamics, Springer, 2018, pp. 400-411.

[24] L. Hou, H. Chen, Y. Chen, K. Lu, Z. Liu, Bifurcation and stability analysis of a nonlinear rotor system subjected to constant excitation and rub-impact, Mechanical Systems and Signal Processing, 125 (2019) 65-78.

[25] R.V. Moreira, A. Paiva, The Influence of Friction in Rotor-Stator Contact Nonlinear Dynamics, in: International Conference on Rotor Dynamics, Springer, 2018, pp. 428-441.

[26] J. Hong, P. Yu, D. Zhang, Y. Ma, Nonlinear dynamic analysis using the complex nonlinear modes for a rotor system with an additional constraint due to rub-impact, Mechanical Systems and Signal Processing, 116 (2019) 443-461.